JAAS

Fluorine-Selective Post-Plasma Chemical Ionization for Enhanced Elemental Detection of Fluorochemicals

Journal:	*Journal of Analytical Atomic Spectrometry*
Manuscript ID	JA-ART-12-2022-000430.R1
Article Type:	Paper
Date Submitted by the Author:	26-Jan-2023
Complete List of Authors:	Tanen, Jordan; Georgetown University, Chemistry White, Samuel; Georgetown University, Ha, Duong; Georgetown University, Chemistry Jorabchi, Kaveh; Georgetown University, Chemistry

Fluorine-Selective Post-Plasma Chemical Ionization for Enhanced Elemental Detection of Fluorochemicals

Jordan L. Tanen, Samuel R. White, Duong Ha, and Kaveh Jorabchi*

Department of Chemistry, Georgetown University, Washington, DC 20057

*Corresponding author: kj256@georgetown.edu

Abstract

Elemental analysis of fluorochemicals has received a renewed attention in recent years stemming from increased use of fluorinated compounds. However, fundamental drawbacks of in-plasma ionization have hindered ICPMS applications in this area. Recently, we have introduced post-ICP chemical ionization for BaF^+ formation using Ba-containing reagent ions supplied by nanospray, leading to major improvements in F detection sensitivity. Here, we present further insights into this post-plasma chemical ionization. First, we examine the effect of oxygen introduced into the plasma (a necessity for organic solvent introduction) on BaF^+ ion formation. The results indicate that excess plasma oxygen leads to abundant HNO_3 in post-plasma flow, shifting ionization reactions toward $BaNO_3^+$ formation and suppressing BaF^+ sensitivity. To amend this, we utilize reagent ions with other metal centers to impart selectivity toward F detection. Our investigations show that robustness of F detection in the presence of abundant HNO_3 improves with the order Al^{3+}~Sc^{3+}>La^{3+}>Mg^{2+}>Ba^{2+} as the metal center in the reagent ions, consistent with stronger metal-F bond in the series. Sc-based ionization resulting in $ScNO_3F^+$ shows the best balance between sensitivity and robustness in the presence of nitric acid. Similarly, this ion shows an improved tolerance relative to BaF^+ for Cl-containing matrix where HCl interferes with ionization. Finally, we demonstrate a unique feature of post-plasma chemical ionization for real-time flagging of matrix effects via monitoring reagent ions. These findings provide significant improvements of post-plasma chemical ionization for elemental F analysis, particularly for online chromatographic detection where solvent gradients are utilized.

Introduction

Fluorochemicals have become ubiquitous over the past decades, as they have found use among several industries and scientific disciplines. For example, organofluorides are increasingly prevalent in today's drug market,[1] the agrochemical industry,[2] and in hole transport layers for photovoltaic solar cells.[3] The increased prevalence of fluorochemicals, as well as their potential toxicity,[4] have created a need for understanding the fate of these compounds in environment and living organisms. Notably, quantitative analysis of these compounds is difficult as standards are not available for many compounds, especially for the biological and environmental transformation products. Elemental methods coupled with chromatography are attractive approaches for such analyses since the fluorine atom acts as a quantitative tag without regard to the compounds' chemical structure.[5]

Inductively coupled plasma mass spectrometry (ICPMS) is often used for elemental speciation but F determination using this technique is hindered by the high ionization potential of fluorine (17.42 eV),[6] resulting in low ionization yield of F to F^+ (9×10^{-4} % at 7500 K).[7] This limitation along with susceptibility of F^+ to space charge effect and reduced ion transmission efficiency lead to a significantly lower sensitivity for F^+ (0.03 cps/(ng/mL))[8] compared to that of metals such as In^+ with a sensitivity $>1\times10^6$ cps/(ng/mL).[9] Formation of fluorine-containing polyatomic ions in the plasma has been pursued to address the poor sensitivity for F with ICPMS.[10–12] For example, addition of barium to ICP yields BaF^+ when fluorinated compounds are introduced into the plasma.[10,11] This has improved F detection sensitivity to 1.6-3.2 cps/(ng/mL),[11,13] allowing for the implementation of this method in several applications.[12–14] Notably, BaF^+ is only detected within a narrow range of aerosol gas flow rates,[11,12] indicating tightly competing factors in ion formation (e.g. simultaneous formation of Ba^{2+} and F^- in plasma) that limit achievable sensitivity.

To improve F detection sensitivity with ICP, we have developed a new approach where the plasma is sampled into a cool atmospheric-pressure recombination zone for formation of F-specific neutral species, which subsequently undergo chemical ionization.[5,15,16] Consequently, in-plasma ion formation constraints are alleviated, resulting in substantially improved sensitivities. For example, a sensitivity of 180 cps/(ng/mL) F was observed by post-plasma formation of Na_2F^+ upon co-introduction of sodium and fluorochemicals into the plasma.[15] Further, this sensitivity was maintained across a wide range of aerosol gas flow rates, indicating reduced effect of plasma temperature on post-plasma ion formation, in contrast to that observed for in-plasma ionization.[11,12] Subsequently, we utilized nanospray with barium acetate electrolyte to supply barium-based reagent ions to the post-plasma flow rather than introducing the metal into the plasma to further control the ionization reactions.[16] A sensitivity of 281 cps/(ng/mL) F was achieved using this post-plasma BaF^+ formation method.[16] The potential of this approach was further demonstrated by coupling it to reversed phase liquid chromatography (LC),[5] resulting in on-column detection limits of 5-12 pmol F compared to in-plasma BaF^+ methods with on-column limits of detection (LODs) >100 pmol F.[14,17] Moreover, quantitation of drug metabolites without species-specific standard was demonstrated by this method, enabling the application of F speciation in drug development.[5]

On the other hand, post-plasma chemical ionization is susceptible to chemical interferences. For example, the BaF^+ signal detected from organofluorines via post-ICP nanospray-induced chemical ionization was suppressed by 32% in the presence of 246 μM Cl as organochlorines in the sample.[16] This was attributed to competition between BaF^+ and $BaCl^+$ formation in the post-plasma flow. Moreover, our recent studies have shown that the amount of

oxygen introduced into the plasma significantly affects F detection sensitivity in post-plasma BaF^+ formation.[5] Notably, introduction of oxygen into the ICP is necessary to prevent the deposition of carbon onto surfaces downstream of the plasma when organic solvents are used. Therefore, a synchronized tuning of oxygen flow rate with solvent gradient was necessary for coupling this technique to gradient LC.[5]

The goal of the current investigation is to enhance robustness of F detection in post-plasma chemical ionization and to minimize the chemical interferences via developing F-specific ionization reactions. Introduction of reagent ions to the post-plasma flow by a nanospray offers a facile way to control the ionization reactions as previously demonstrated by sodium and barium-based ionizations.[16] In this work, the nature of chemical interference on F detection is further explored and several other metal centers selected based on their physicochemical properties are investigated to improve post-ICP ionization selectivity and robustness.

Experimental

Sample Preparation

Nanospray solutions were prepared from solid salts of sodium acetate trihydrate (Fisher Scientific, Fairlawn, NJ), barium nitrate, cesium nitrate, magnesium nitrate hexahydrate, scandium nitrate hydrate, aluminum nitrate nonahydrate (all from Sigma-Aldrich, Milwaukee, WI), and lanthanum nitrate (Strem Chemicals, Newburyport, MA) dissolved in 18.2 MΩcm water. All nanospray solutions were prepared to a concentration of 1 mM. Solid samples of fluconazole and sucralose (Sigma-Aldrich, Milwaukee, WI) were prepared in a 50:50 water:acetonitrile solvent containing 0.1% v/v formic acid to mimic a typical reversed phase LC solvent.

Instrumental Setup

Sample solutions were introduced by flow injections through a 20-μL injection loop, carried by a 50:50 water:acetonitrile solvent with 0.1% v/v formic acid at a flow rate of 50 μL/min. The sample was aerosolized by a nebulizer (HEN-90-A0.1, Meinhard, Co) into a cyclonic spray chamber (Meinhard, CO) using 1.4 L/min argon gas. The aerosol was then mixed with oxygen using a tangential mixer (Meinhard, CO). The oxygen flow rate was electronically controlled by a valve (Porter EPC, Parker Hannifin Corp, Hatfield, PA) placed upstream of a 100 μm i.d. capillary to restrict flow to the 10-50 mL/min range. An Arduino microcontroller board (Due, Somerville, MA) supplied the voltage to the valve with voltage values calibrated using a bubble flowmeter. An ICP torch injector with a 2 mm internal diameter (i.d.) was used, and the plasma was operated at 1300 W RF power setting using a NexIon ICP generator (PerkinElmer, Waltham, MA) with 14 and 1.2 L/min of plasma and auxiliary gas flow rates, respectively.

An improved post-plasma chemical ionization interface was developed to allow further control of plasma flow sampling and downstream ionization reactions as depicted in **Figure 1**. The interface was composed of two chambers both operating at atmospheric pressure and connected via a steel tube supported within an aluminum disk (5" diameter and 0.5" thick). The second chamber was sealed to the sampling plate of the MS and was vacuum pumped at the rate of 4 L/min, monitored by a mass flow meter (Sierra Instruments, Monterey, CA) and controlled by a needle valve connected to vacuum. A flow of zero grade air was introduced into the first chamber.

The balance between the pumping rate of the second chamber and the air flow rate introduced into the first chamber determined the extent of plasma sampling into the chemical ionization interface.

The first chamber was encased in an acrylic tube (58 mm × 2 in. outer diameter (o.d.) ×1¾ i.d.) pressed against an aluminum disk (on the left side) which itself was pressed against a water-cooled aluminum plate (PerkinElmer, Waltham, MA). The aluminum plate held a 4-mm nickel sampler (Spectron, Ventura, CA). The sampler was placed 10-11 mm downstream of the ICP load coil. The plasma flow passing through the nickel sampler traveled through a quartz tube (57 mm × ¼" o.d. × 4 mm i.d.) where plasma cooling and recombination reactions occurred. The end of the tube was suited with either a cylindrical or a parallel plate brass electrode held at 400 V to produce a well-defined electric field between the end of the recombination tube and the steel tube to guide ions and to avoid charging of the quartz tube.

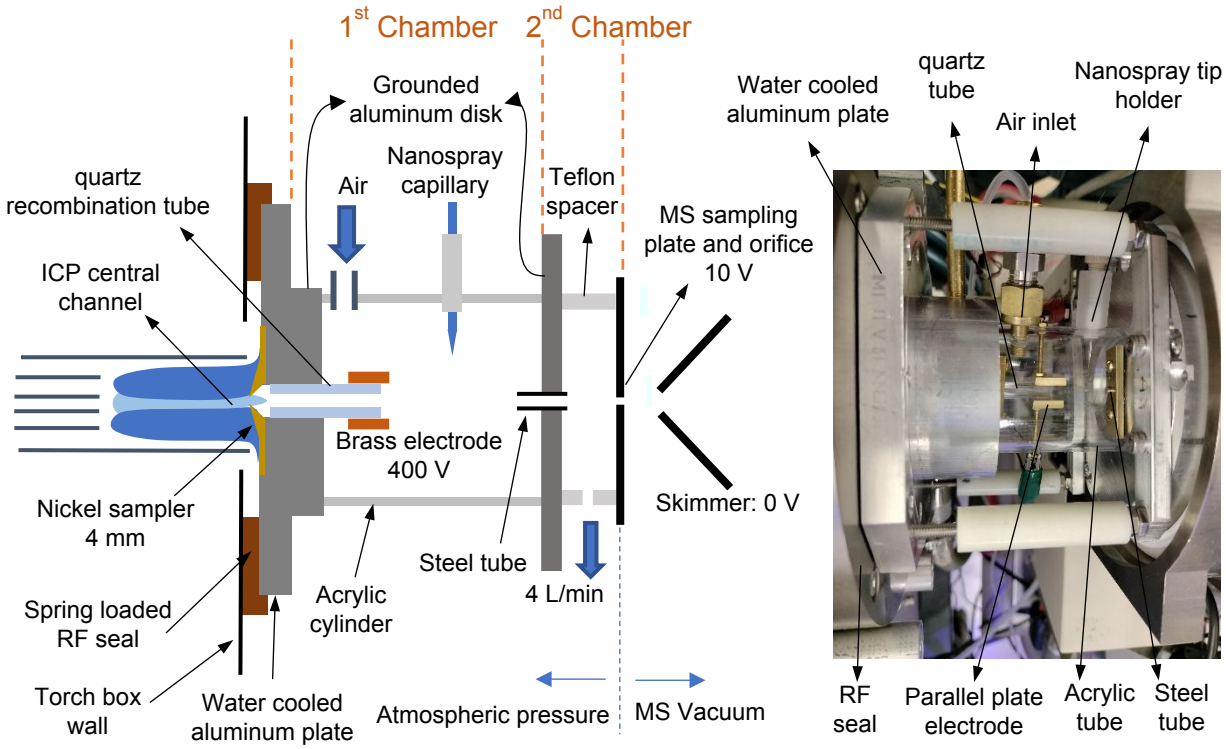

Figure 1. Schematic diagram of the post-plasma chemical ionization interface on API3000 mass spectrometer and a picture of the first chamber of the interface. The second chamber is behind the aluminum plate and is not visible in the photograph.

The reagent ions were introduced using a nanospray placed perpendicular to the post-plasma flow with the tips ~1 cm downstream of the brass electrode and 7 mm from the central axis of the quartz tube. The nanospray tips were made of borosilicate capillaries (1 mm o.d., 0.75 mm i.d.) pulled using a micropipette puller to ~5 µm i.d. and loaded with aqueous solutions of electrolytes. The spray capillary was secured by a union fitting threaded to the acrylic cylinder encasing the first chamber. The nanospray ionization process was controlled by applying 1200-1300 V to a platinum wire inserted in the back of the nanospray tip. The post-plasma flow along

with the ions from nanospray was pulled from the first chamber into the second chamber through a grounded steel tube (27 mm × 1/8" o.d. and 2 mm i.d.), ensuring efficient mixing of nanospray ions and post-plasma neutral species for enhanced ionization efficiency and stability of signal. The entrance of the steel tube was located 12 mm downstream of the nanospray tip while the end of the steel tube was 9 mm away from the MS sampling orifice. Ions were sampled into a triple quadrupole MS (API 3000, Sciex, Framingham, MA) with soft conditions (declustering potential (DP) of 10 V) to minimize the dehydration and fragmentation.

The F-containing ions formed in the post-plasma area are referred to as analytical ions in this work. The zero-grade air flow rate into the first chamber was optimized by maximizing the analytical ion intensity while minimizing the peak shape factor, defined as the peak area-to-height ratio. Unless noted otherwise, the analytical ions were detected in Q1 single ion monitoring (SIM) mode with 200 ms dwell time each. The background ion scans were acquired from 20 to 500 m/z with 0.1 m/z increments over a scan time of 2 seconds. In the event that any background ion intensity exceeded the detector's limit of linearity (~$2x10^6$ cps), ions were defocused by adjusting the focusing lens potential between Q1 and Q2 from -12 to -9 V, reducing the ion flux. The resulting spectra were then corrected after data acquisition. The correction factor was obtained by measuring the ratio of intensities with focused vs defocused detection monitoring an ion whose intensity did not exceed 10^6 cps when the ion flux was not reduced. The "corrected ion intensity" term denoted in the spectra refers to this correction.

Ion Hydration

It is of note that the curtain gas normally desolvating ions upstream of the MS sampling orifice is eliminated in the double chamber design described above, leading to higher hydration of detected ions. While this may create analytical disadvantages because of distribution of ion intensity between various hydration levels of analytical ions, it is advantageous for fundamental studies because the detected ions more closely reflect the original hydration status of the ions during their reactions with the post-plasma neutrals.

To determine the representative hydration levels for F-containing ions, m/z values corresponding to ions with 1-7 water molecules (i.e. $A(H_2O)_{1\text{-}7}^+$ where A stands for the core ion) were monitored in SIM mode using flow injections of fluconazole. The ions accounting for > 95% of the total hydrated ion intensity were then identified and their intensity summation was used for the studies reported below. The same 95% metric was applied for identifying and summing the intensities of hydrated background ions in the scanned spectra.

Results and Discussion

Nitric acid formation by excess oxygen in the plasma and its effect on BaF^+ formation

Our investigations first focused on understanding the effect of oxygen introduced into the plasma on BaF^+ formation. This ion is detected with good sensitivity upon flow injections of fluorinated compounds into the ICP when barium-based electrolyte is used in nanospray,[16] but a tight control of oxygen amount in the plasma is needed for efficient formation BaF^+.[5]

Figure 2 illustrates the drastic effect of oxygen flow rate introduced into the plasma on BaF^+ detection using sensitivity (Eq. 1) as a metric for F detection efficiency:

$$\text{Sensitivity} = \frac{\text{Flow injection peak height}}{\text{F concentration}} \qquad \text{(E1)}$$

At the low oxygen flow rate of 10 mL/min, $BaF(H_2O)_{1\text{-}3}^+$ ions are detected with total sensitivity > 600 cps/(ng/mL), far better than 2-3.2 cps/(ng/mL) reported in ICPMS/MS experiments.[11,12] However, the $BaF(H_2O)_{1\text{-}3}^+$ sensitivity is reduced precipitously as the oxygen flow rate is increased. Concurrently, we observe a rapid rise in $BaNO_3(H_2O)_{2\text{-}4}^+$ as shown in **Figure 2**, suggesting a potential role of plasma-produced nitrate-containing species in BaF^+ ion suppression.

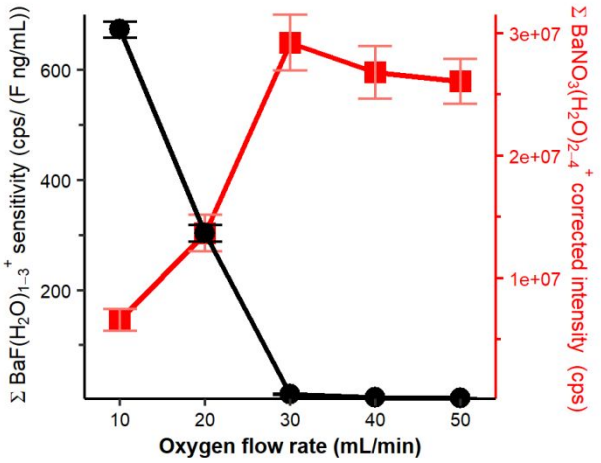

Figure 2. Effect of oxygen flow rate introduced into the ICP on total $BaF(H_2O)_{1\text{-}3}^+$ sensitivity and total $BaNO_3(H_2O)_{2\text{-}4}^+$ intensity. Sensitivity was measured by flow injections of 99.8 μM F in the form of fluconazole, error bars represent standard deviation based on triplicate injections. Error bars for $BaNO_3(H_2O)_{2\text{-}4}^+$ intensities represent standard deviations of intensity based on scans acquired over 30 seconds.

The rising prominence of $BaNO_3(H_2O)_n^+$ is further depicted in **Figure 3** with the background ion spectra at three different experimental conditions. When the plasma is off and the ionization interface is flushed using zero grade air (**Figure 3A**), the nanospray predominantly produces $Ba(H_2O)_n^{2+}$ and $BaNO_3(H_2O)_n^+$. The hydrated doubly charged ions constitute the majority of the total intensity of these barium-containing ions originating from nanospray. When the plasma is turned on (10 mL/min oxygen along with solvent) and the air flow rate to the interface is adjusted to the optimal plasma sampling for F detection, $Ba(H_2O)_n^{2+}$ ions are drastically reduced in intensity while new species such as $BaHCO_2(H_2O)_n^+$ and $BaNO_2(H_2O)_n^+$ are detected in addition to $BaNO_3(H_2O)_n^+$ as illustrated in **Figure 3B**. Finally, **Figure 3C** depicts that at a higher oxygen flow rate of 50 mL/min, $BaNO_3(H_2O)_n^+$ ions near-exclusively represent the barium species in the spectrum, illustrating the dominance of nitrate-containing species in the post-plasma flow.

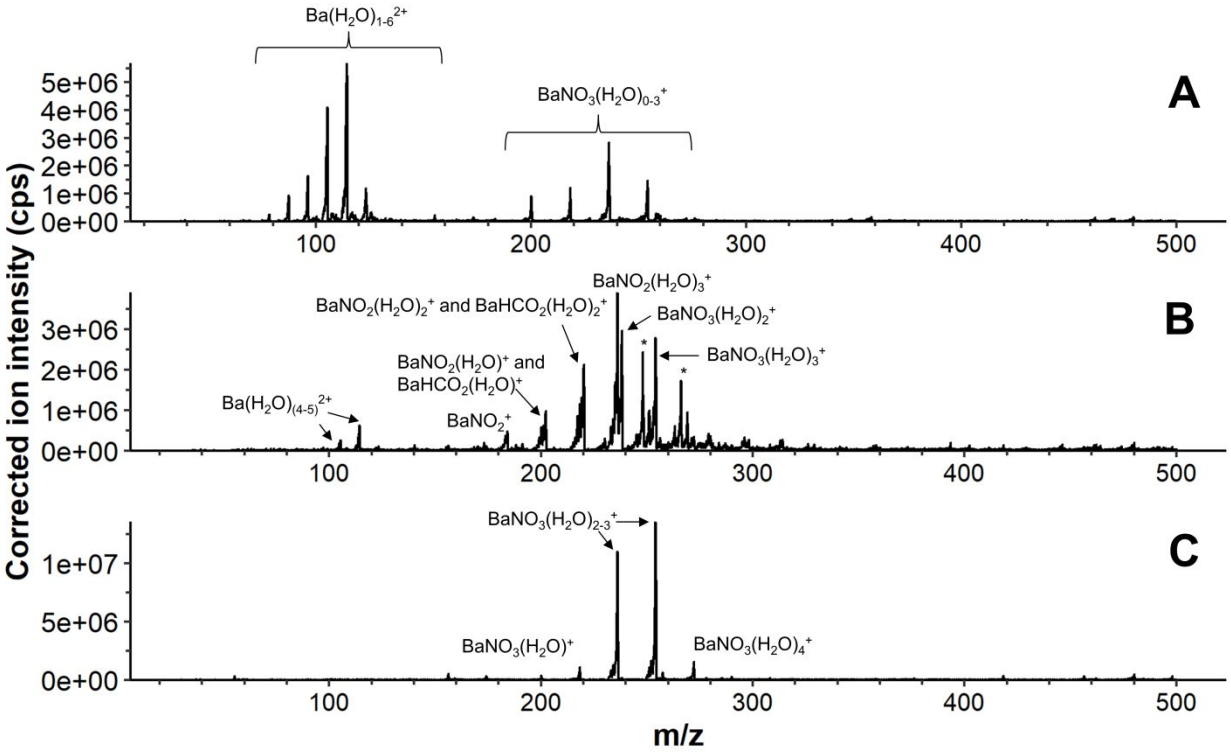

Figure 3. (A) Nanospray ions produced from a 1 mM $Ba(NO_3)_2$ solution with plasma off and 3.3 L/min of air delivered into the reaction interface. (B) and (C) show ions detected upon nanospray ion interactions with plasma afterglow at an oxygen flow rate of 10 mL/min, and 50 mL/min, respectively. For (B) and (C) the air flow rate was lowered to 2.6 L/min for optimal detection of F from flow injection of a 100 μM fluconazole sample. Peaks with (*) signs indicate unidentified species.

The rise of $BaNO_3(H_2O)_n^+$ could originate from reactions of nanospray ions with two species in the post-plasma flow generated at higher oxygen flow rates: 1) NO_3^- and 2) HNO_3. The former would convert $Ba(H_2O)_n^{2+}$ to $BaNO_3(H_2O)_n^+$ while neutralizing the singly charged ions. The latter leads to ion-neutral reactions that could convert all ions to $BaNO_3(H_2O)_n^+$ without loss of total ion intensity.

To evaluate the relative importance of the two species, we changed the nanospray solution and created only singly-charged ions where ion-ion reactions would lead to neutralization and loss of intensity as discussed above. 10 mM sodium acetate solution was used for this purpose instead of the barium nitrate solution. **Figure 4** depicts a difference spectrum where the spectrum obtained with plasma sampling at interface air flow rate of 2.6 L/min was subtracted from that obtained at an air flow rate of 5.6 L/min to block plasma sampling. Singly-charged clusters of $Na(NaCH_3CO_2)_n^+$ are evident in positive intensities when the plasma is excluded from the interface while these clusters are converted to $Na(NaNO_3)_n^+$ upon plasma sampling, evident in negative intensities.

Notably, the total $Na(NaNO_3)_n^+$ intensity upon plasma sampling (negative intensities in **Figure 4)** is only 16 % larger than the total $Na(NaCH_3CO_2)_n^+$ intensity (positive intensities in **Figure 4**). The slight increase in total intensity may result from changes in ion transmission

efficiencies even though the nitrate and acetate clusters are close to each other in mass. This lossless conversion of singly-charged $Na(NaCH_3CO_2)_n^+$ to $Na(NaNO_3)_n^+$ ions indicates that contribution of NO_3^- is negligible in the conversion. The spectra with and without plasma sampling are also shown in Figure S1 of the Electronic Supporting Information, depicting disappearance of $Na(NaCH_3CO_2)_n^+$ upon plasma sampling. In other words, $Na(NaCH_3CO_2)_n^+$ ions are converted to $Na(NaNO_3)_n^+$ in a near-complete fashion upon plasma sampling.

Effect of negative ions from the plasma was also tested using cesium nitrate as the nanospray solution shown in Figure S2. This solution produces a simpler spectrum where the ions do not react effectively with HNO_3 but are expected to react with negative ions because of immensely favorable reactions of oppositely charged ions in the gas phase. Similar to the cluster ions discussed above, the total intensity of cesium ions does not change appreciably with and without plasma sampling, confirming negligible effect of negative ions from plasma on ion formation in nanospray-induced post-plasma chemical ionization.

In sum, the near-complete conversion of singly charged cluster ions and negligible presence of negative ions imply that introduction of oxygen into the plasma at high flow rates results in a substantial concentration of HNO_3 in post-plasma flow, leading to collisions of all ions with HNO_3 prior to detection by the MS.

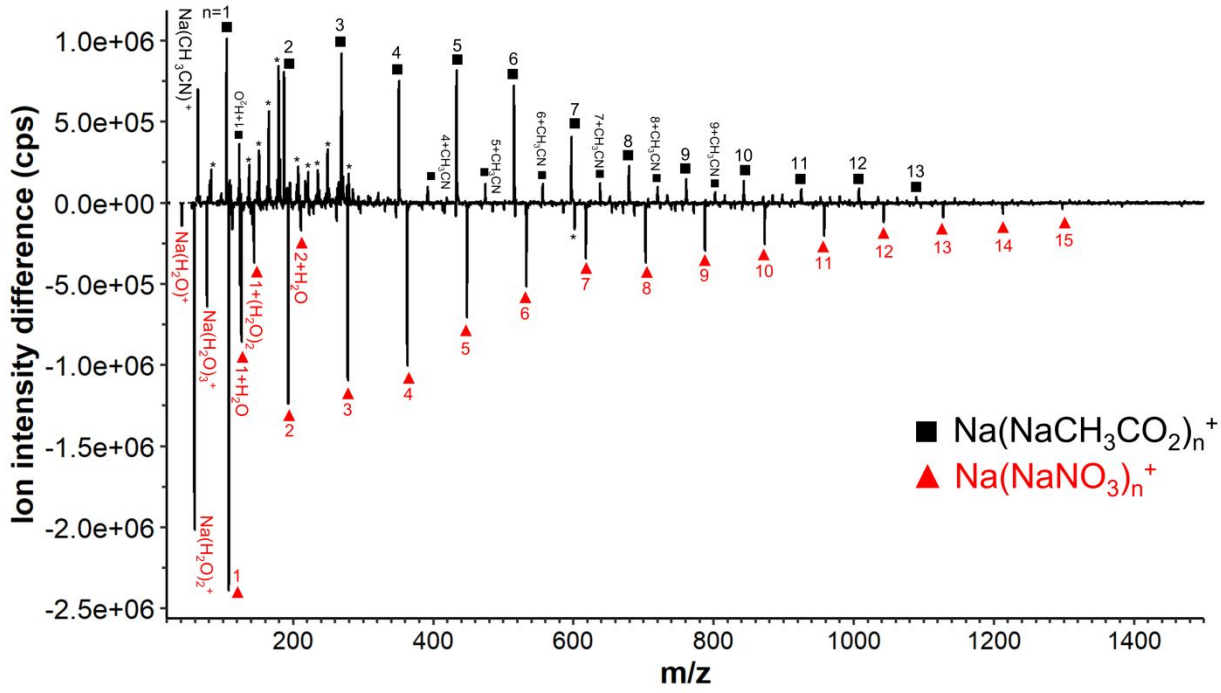

Figure 4. Difference spectrum using 10 mM $NaCH_3CO_2$ as nanospray electrolyte, depicting the effect of plasma sampling on singly charged clusters. Positive intensities represent ions detected when the plasma is excluded from the interface (5.6 L/min air flow rate) while negative intensities represent ions that appear in the spectrum when the plasma is sampled into the interface (2.6 L/min air flow rate). Peaks marked with (■) represent clusters of $Na(NaCH_3CO_2)_n^+$, with n denoting the cluster size. Peaks marked with (▲) represent clusters of $Na(NO_3)_n^+$. Peaks with (*) signs indicate unidentified species. O_2 flow rate of 50 mL/min was used for these studies. Both background scans acquired with a scan time of 3 seconds.

This high concentration of HNO_3 produced at 50 mL/min of oxygen in the plasma explains BaF^+ sensitivity loss via R1 when these ions encounter HNO_3:

$$BaF(H_2O)_n{}^+{}_{(g)} + HNO_{3(g)} \rightleftarrows BaNO_3(H_2O)_n{}^+{}_{(g)} + HF_{(g)} \qquad (R1)$$

Our previous density functional theory (DFT) calculations for n = 0 have shown a thermodynamically favorable reaction with ΔH_{298K} = -18.7 kJ/mol for R1,[16] further supporting that $HNO_{3(g)}$ would suppress the analytical signal of BaF^+.

The loss in BaF^+ sensitivity can also be explained from the perspective of ionization (reverse of reaction R1) as opposed to neutralization of the analytical ion. At high oxygen flow rates, $BaNO_3(H_2O)_n{}^+$ ions are the only species in the background spectrum (**Figure 3C**). Thus, these ions would be the only reagent ions available for the ionization and formation of F-containing ions. To form BaF^+, $BaNO_3(H_2O)_n{}^+$ ions would have to react with HF produced in the post-plasma flow from injections of organofluorines. In other words, the reverse of R1 would be the ionization reaction of interest. Low sensitivity for BaF^+ at high oxygen levels suggests that R1 does not proceed in the reverse direction stemming from high $HNO_{3(g)}$ concentrations and a thermodynamically unfavorable reaction indicated by the computational results noted above. With the identification of $HNO_{3(g)}$ as a major chemical interferent, we evaluated alternative ionization pathways to improve F detection robustness as discussed below.

Table 1. Physicochemical properties of metal ions.

Metal ion	Ionic radius (Å)	Hardness[a]	$\log(K_{Association})$ between F^- and M^{n+} in solution (μ= 0.5 M)	Background electrolyte used in $K_{Association}$ measurement
Ba^{2+}	1.35	12.8	-0.09 (ref. 18)[b]	0.5 M $NaClO_4$
Mg^{2+}	0.72	32.5	1.30 (ref. 18)	0.5 M $NaClO_4$
La^{3+}	1.03	15.4	2.78 (ref. 19)	0.5 M NaCl
Sc^{3+}	0.75	24.6	6.18 (ref. 20)	0.5 M $NaClO_4$
Al^{3+}	0.54	45.8	6.13 (ref. 20)	0.53 M KNO_3

[a] Hardness is calculated from ½(I – E), where I and E are the ionization potential and electron affinity of M^{n+}, respectively.[21] Ionization potentials, electron affinities, and ionic radii are taken from CRC.[6]
[b] Association constant for Ba^{2+} to fluoride is an upper estimate, as the actual value was not measurable with the method used.[18]

Effect of metal center in reagent ions on F detection robustness

To prevent reaction of the analytical ion with $HNO_{3(g)}$ in R1 (or to promote reverse of R1 for ionization), the reactants in R1 must become more stable relative to the products. One approach to achieve this goal is to improve the metal-F bond strength in the analytical ion. Considering the small radius of fluorine and its high electronegativity, the metal-F bond is expected to have a significant ionic characteristic. Therefore, we sought to strengthen this bond by using metals with

higher charge states and smaller radii to enhance the electrostatic interaction of fluorine with the metal center in the analytical ion.

We first set the conditions to keep the metal ion charge constant while utilizing an ion with a smaller radius. Mg is the logical choice in this regard belonging to group 2 of periodic table similar to Ba but with drastically smaller ionic radius (See **Table 1**). Using 1 mM $Mg(NO_3)_2$ solution as nanospray electrolyte and a plasma oxygen loading of 10 mL/min, $MgF(H_2O)_{3\text{-}4}^+$ ions were detected upon injection of fluconazole. **Figure 5A** depicts the effect of plasma oxygen flow rate on Mg-based ionization, illustrating that total $MgF(H_2O)_{3\text{-}4}^+$ sensitivity decreases as a function of O_2 flow rate while a concurrent rise in $MgNO_3(H_2O)_n^+$ ion intensity is observed. Moreover, at an oxygen flow rate of 50 mL/min $MgNO_3(H_2O)_n^+$ ions are the dominant species detected by the MS (**Figure 5B**). These results are similar to behavior of barium-based ionization **(Figures 2 and 3C)** and denote the suppression of $MgF(H_2O)_{3\text{-}4}^+$ in the presence of HNO_3.

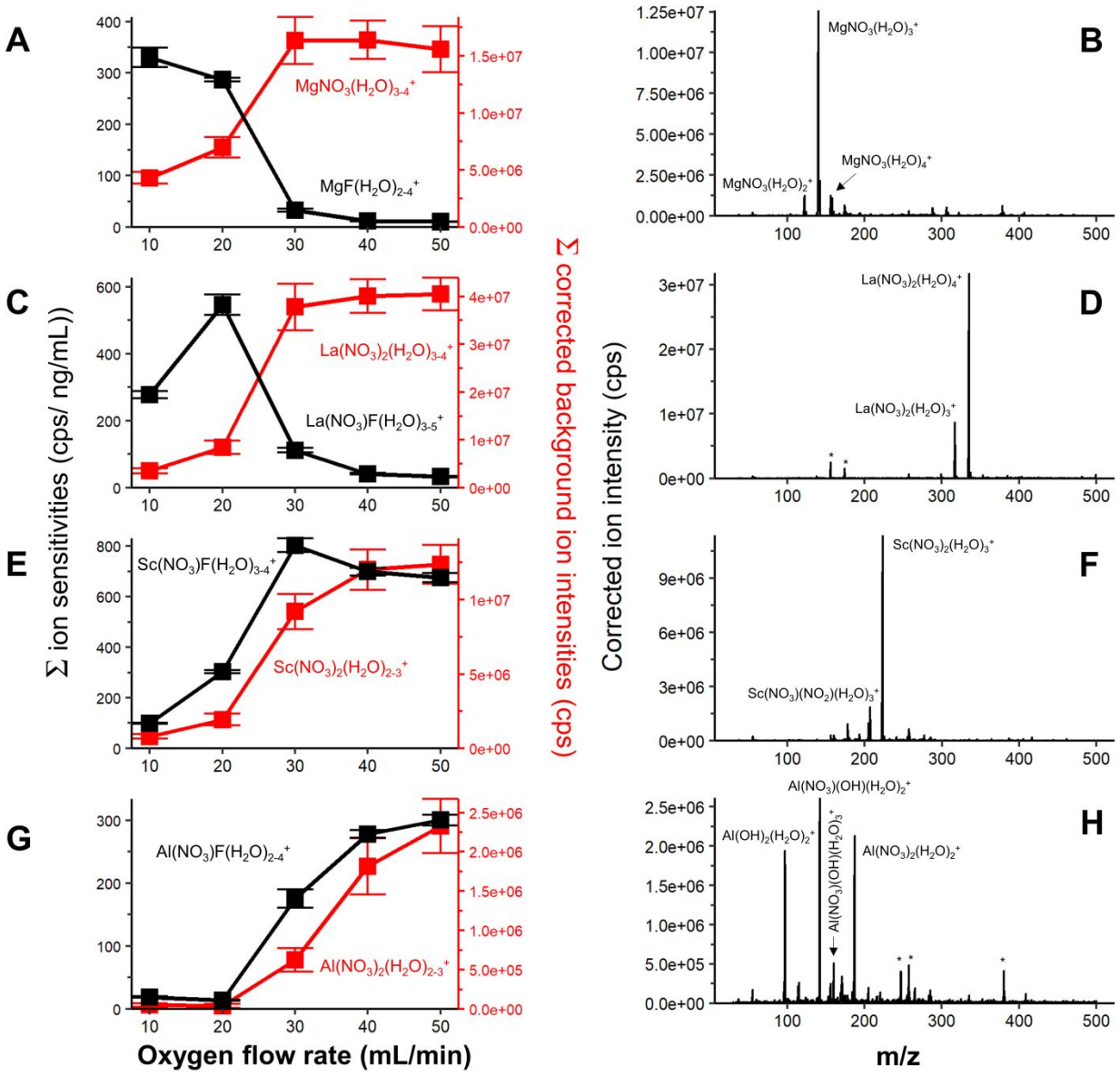

Figure 5. (A, C, E, G) Effect of oxygen flow rate on F detection and intensities of nitrate-containing ions. Black lines show F detection sensitivity (summed over hydrated analytical ions) based on flow injections of 99.8 μM F from fluconazole samples, and error bars represent the standard deviation of triplicate measurements. Red lines depict combined ion intensities for $M(NO_3)(H_2O)_n^+$ and $M(NO_3)_2(H_2O)_n^+$ ions, error bars represent the standard deviations of intensity based on scans acquired over 30 seconds. (B,D,F,H) Ions detected upon interactions of nanospray ions with the post-plasma flow using at 50 mL/min plasma oxygen loading. All data were acquired using an air flow rate of 2.6 L/min. Peaks with (*) signs indicate unidentified species.

However, $MgF(H_2O)_{3\text{-}4}^+$ sensitivity reduction in **Figure 5A** is not as steep as that of $BaF(H_2O)_{1\text{-}3}^+$ in **Figure 2**. Relative to the sensitivity at 10 mL/min O_2, the $MgF(H_2O)_{3\text{-}4}^+$ sensitivity decreases by 15% ± 5% and 90% ± 0.9% at 20 and 30 mL/min O_2, respectively. In contrast, $BaF(H_2O)_{1\text{-}3}^+$ sensitivity undergoes reductions of 55% ± 2.5% and 98% ± 0.1% at 20 and 30 mL/min O_2, respectively, relative to that at 10 mL/min (**Figure 2**). This observation suggests an improved robustness and higher resilience of $MgF(H_2O)_{3\text{-}4}^+$ toward reactions with HNO_3. Nevertheless, the interference from HNO_3 is still severe at high oxygen levels, indicating that Mg-based ionization is not a sufficiently robust ionization route for F detection.

To examine the effect of metal center charge, we selected La, Sc, and Al, which offer trivalent metals with progressively smaller ionic radii (see Table 1). **Figure 5C** illustrates that using 1 mM $La(NO_3)_3$ solution in nanospray, $La(NO_3)_2(H_2O)_n^+$ ions increase in intensity as a function of oxygen flow rate introduced into the plasma. These ions become the dominant species in the spectrum at 50 mL/min of oxygen as depicted in **Figure 5D**. Considering the dominance of $La(NO_3)_2(H_2O)_n^+$ at high oxygen flow rates, we monitored $LaFNO_3(H_2O)_{3\text{-}5}^+$ as analytical ions with potentially improved tolerance to HNO_3. **Figure 5C** shows that the sensitivity for these ions peaks at a respectable value of 550 cps/(ng/mL) at an oxygen flow rate of 20 mL/min. However, the $LaFNO_3(H_2O)_{3\text{-}5}^+$ sensitivity undergoes a reduction at higher oxygen flow rates while the intensity of $La(NO_3)_2(H_2O)_n^+$ continually increases. The reduction in $LaFNO_3(H_2O)_{3\text{-}5}^+$ sensitivity in **Figure 5C** from the highest value to that at 50 mL/min is 94% ± 0.5%, while these values are 99% ± 0.7% and 97% ± 0.3% for Ba- (**Figure 2**) and Mg-based (**Figure 5A**) ionization, respectively. These trends show an improved robustness of ionization using La relative to Mg and Ba as expected from its higher charge.

The behavior of Sc-based ionization is summarized in **Figures 5E** and **5F** using nanospray of 1 mM scandium nitrate solution. $Sc(NO_3)_2(H_2O)_n^+$ species increase as a function of oxygen flow rate introduced into the plasma (**Figure 5E**), becoming dominant at 50 mL/min (**Figure 5F**). Interestingly, the sensitivity for the analogous analytical ions, $ScNO_3F(H_2O)_{3\text{-}4}^+$, follows a similar general trend as that of $Sc(NO_3)_2(H_2O)_n^+$ in **Figure 5E** and only decreases slightly at higher oxygen flow rates (15% ± 4% from 30 to 50 mL/min O_2), suggesting a significantly improved resilience to HNO_3 interference.

Finally, **Figures 5G** and **5H** depict the behavior of aluminum-based ionization using 1 mM aluminum nitrate as nanospray solution. At a higher oxygen flow rate of 50 mL/min, $Al(OH)_2(H_2O)_n^+$, $AlOHNO_3(H_2O)_n^+$, and $Al(NO_3)_2(H_2O)_n^+$ are dominant species in the spectrum of **Figure 5H**. Given the steady increase of $Al(NO_3)_2(H_2O)_n^+$ intensity with oxygen flow rate in **Figure 5G**, we selected $AlNO_3F(H_2O)_{2\text{-}4}^+$ as potential analytical ions. **Figure 5G** also illustrates that the sensitivity for $AlNO_3F(H_2O)_{2\text{-}4}^+$ continually increases with oxygen flow rate, providing the highest robustness for F detection in the presence of abundant HNO_3.

In summary, the trends in sensitivity as a function of plasma oxygen load illustrated in **Figures 2** and **5** offer a qualitative picture of increasing robustness for F detection in the order of $Ba^{2+} < Mg^{2+} < La^{3+} < Sc^{3+} < Al^{3+}$ for the metal centers in the analytical ions.

Quantitative robustness comparison via reagent ion reactivities at high oxygen level

To obtain a more quantitative comparison among the various metal centers for F detection in the presence of interfering HNO_3, we further evaluated the ion formation at high oxygen flow rate of 50 mL/min. At these conditions, the background ions are dominated by nitrate-containing species as discussed above. Consequently, these background ions may be considered as reagent ions for reactions with HF to produce $MF(H_2O)_n^+$ and $MFNO_3(H_2O)_n^+$ for divalent and trivalent metals, respectively, as shown in Reactions R2-R5:

$$MNO_3(H_2O)_n{}^+{}_{(g)} + HF_{(g)} \rightleftarrows MF(H_2O)_n{}^+{}_{(g)} + HNO_{3(g)} \quad \text{(R2)}$$

$$MNO_3NO_2(H_2O)_n{}^+{}_{(g)} + HF_{(g)} \rightleftarrows MNO_3F(H_2O)_n{}^+{}_{(g)} + HNO_{2(g)} \quad \text{(R3)}$$

$$M(NO_3)_2(H_2O)_n{}^+{}_{(g)} + HF_{(g)} \rightleftarrows MNO_3F(H_2O)_n{}^+{}_{(g)} + HNO_{3(g)} \quad \text{(R4)}$$

$$MNO_3OH(H_2O)_n{}^+{}_{(g)} + HF_{(g)} \rightleftarrows MNO_3F(H_2O)_n{}^+{}_{(g)} + H_2O_{(g)} \quad \text{(R5)}$$

The reactivities of these reagent ions are then quantified by Equation 2:

$$\text{Reactivity} = \frac{\text{Total sensitivity of hydrated analytical ion}}{\Sigma\ \text{Reagent ion intensities}} \quad \text{(E2)}$$

where $BaF(H_2O)_{1\text{-}3}^+$ and $MgF(H_2O)_{3\text{-}4}^+$ were used as analytical ions for Ba- and Mg-based ionization, while for trivalent metals we used $LaNO_3F(H_2O)_{3\text{-}5}^+$, $ScNO_3F(H_2O)_{3\text{-}4}^+$, and $AlNO_3F(H_2O)_{2\text{-}4}^+$. Corresponding reagent ions that lead to the analytical ions via reaction with HF are described in R2-R5 above. The reactivity as defined by E2 reflects the fraction of reagent ions that are converted to analytical ions per ng/mL of F introduced into the plasma. At a high oxygen flow rate of 50 mL/min, significant HNO_3 is present in the ionization area. Thus, reactivities of various metals measured in this condition quantify the effectiveness of ionization in the presence of interfering HNO_3.

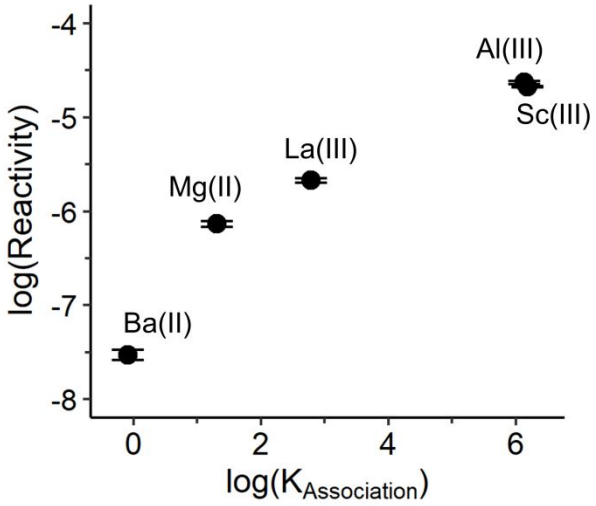

Figure 6. Reactivities of nitrate-containing reagent ions toward HF (quantified by Equation 2) as a function of solution-phase association constant between metal and fluoride ions. Analytical ions were detected upon injection of ~100 μM F from fluconazole at 50 mL/min O_2 flow rate. An air flow rate of 2.6 L/min was used for these experiments.

Figure 6 depicts reactivities in logarithmic scale, illustrating the reactivity order as Ba^{2+} < Mg^{2+} < La^{3+} < Sc^{3+} ~ Al^{3+}, in line with qualitative trends discussed above. To interpret the reactivity trend, the effects of metal center's ionic radius and charge on bonding with F can be considered using ion hardness. Generally, a harder metal would be expected to have a stronger bond with fluorine given the hardness of the fluoride ion. Using half of the difference between ionization energy and electron affinity as a quantitative metric for hardness,[21] **Table 1** shows that the order of reactivities has a positive correlation with hardness, except for Mg(II) which is a hard ion but with low reactivity. While general trends can be predicted by the hardness model, this view is clearly too simplistic to fully capture the reactivities of ions. Interestingly, **Figure 6** shows that reactivities measured in gas phase have a strong correlation with fluoride binding affinities measured for metals in aqueous solutions (**Table 1**). This correlation could indicate that metals retain their major solution characteristics in gas phase as well. Alternatively, one could hypothesize that hydration of ions in gas phase brings the behavior closer to the solution phase trends. As noted above, ions are hydrated during their interactions with the post-plasma flow. The details of hydration effects remain to be studied.

In conclusion, scandium and aluminum-based reagent ions show the greatest reactivity towards HF in the presence of HNO_3. This indicates a selectivity for HF for these metal ions attributed to their small radii and their higher charge. Although Al- and Sc-based ions offer comparable reactivities, we opted to continue the remainder of the studies using scandium-based ions, because of higher sensitivity offered by $ScNO_3F(H_2O)_{3\text{-}4}^+$ for F detection evident in **Figure 5E** versus **5G**.

Matrix effects from Cl using Sc-based ionization for F detection

Encouraged by the robustness of $ScNO_3F(H_2O)_n^+$ detection in the presence of HNO_3, we evaluated the extent of matrix tolerance for these ions in Cl-containing matrices. Such matrices are

expected to produce HCl in post-plasma flow which may pose an interference via reactions with the analytical ion similar to HNO_3 reactions discussed above.

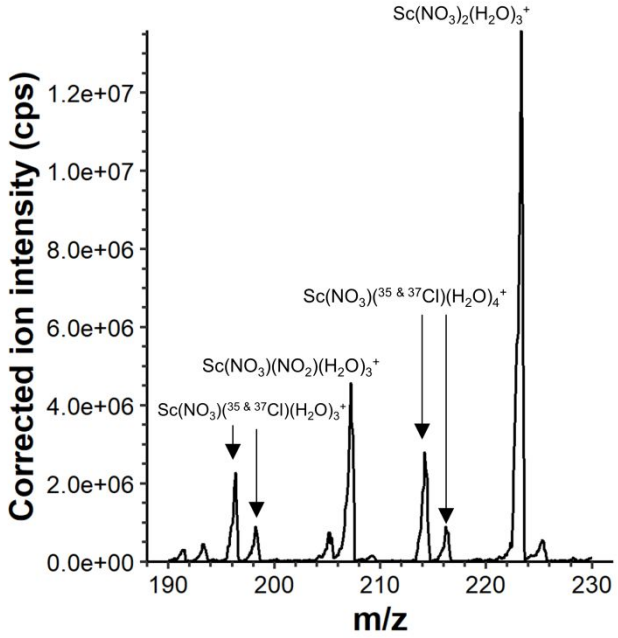

Figure 7. Ions detected upon injection of a 10.1 mM Cl from sucralose using 1 mM $Sc(NO_3)_3$ as nanospray solution. An interface air flow rate of 2.6 L/min and oxygen flow rate of 50 mL/min were used in this experiment.

Figure 7 shows a spectrum detected using Sc-based ionization upon injection of 10.1 mM Cl in the form of sucralose. Significant formation of $ScNO_3Cl(H_2O)_{3\text{-}4}^+$ is evident in the spectrum, indicating reactions of HCl with the reagent ions. Notably, the ^{37}Cl isotope in $ScNO_3Cl(H_2O)_n^+$ ions creates an isobaric interference for $ScNO_3F(H_2O)_{n+1}^+$. Therefore, we utilized a MS/MS detection method to eliminate this isobaric interference in evaluation of Cl-matrix tolerance. $ScNO_3F(H_2O)_4^+$ was selected as the precursor ion because of its highest intensity among other hydrates and was fragmented to $ScFO_2^+$ at a collision energy of 45 eV. A dwell time of 500 ms was used for monitoring the product ion.

Table 2. Matrix effects for detection of F as $ScFNO_3(H_2O)_4^+$

F concentration	Matrix concentration	Normalized response factor
19.1 µM F	Without Cl matrix	100.0 ± 4.9%
20.5 µM F	1.83 mM Cl from sucralose	106% ± 8.1%
19.3 µM F	10.1 mM Cl from sucralose	83.0% ± 3.6%

Air flow rate of 2.6 L/min and O_2 flow rate of 50 mL/min were used for these experiments.

Table 2 summarizes effect of Cl matrix on $ScNO_3F(H_2O)_4^+$ detection using response factor, defined as the flow injection peak area divided by the F concentration. All response factors are normalized to that of the sample without Cl matrix for ease of comparison. No significant matrix effect is observed up to Cl concentration of 1.8 mM while 17% reduction in response factor is detected for a matrix with 10 mM Cl. In contrast, F detection via post-plasma formation of BaF^+

showed 32% suppression from samples with Cl concentrations as low as 246 µM.[16] This substantial improvement in Cl matrix tolerance by the scandium-based ionization is in line with the expectation based on resistance to HNO_3 interference discussed above. However, the matrix effect from Cl is more pronounced in post-plasma chemical ionization compared to that observed for in-plasma formation of BaF^+ in ICP-MS/MS where a suppression of < 10% is reported for 18.7 mM Cl in the form of NH_4Cl.[12]

A unique feature of chemical ionization compared to in-plasma ionization in ICPMS is the presence of reagent ions in the spectra. This offers an opportunity to flag the matrix effects without *a priori* knowledge of the matrix. To examine this possibility, we monitored the primary reagent ion $Sc(NO_3)_2(H_2O)_3^+$ concurrently with $ScNO_3F(H_2O)_4^+$ during flow injections. **Figure 8** shows signals for flow injections of fluconazole with and without Cl matrix spiked into the solution. Notably, a dip in reagent ion intensity is observed in **Figure 8** coincident with the suppression of the analytical signal in the presence of matrix, confirming that the reagent ion monitoring could serve as a rapid way to detect matrix effect and alert the analyst to take corrective measures.

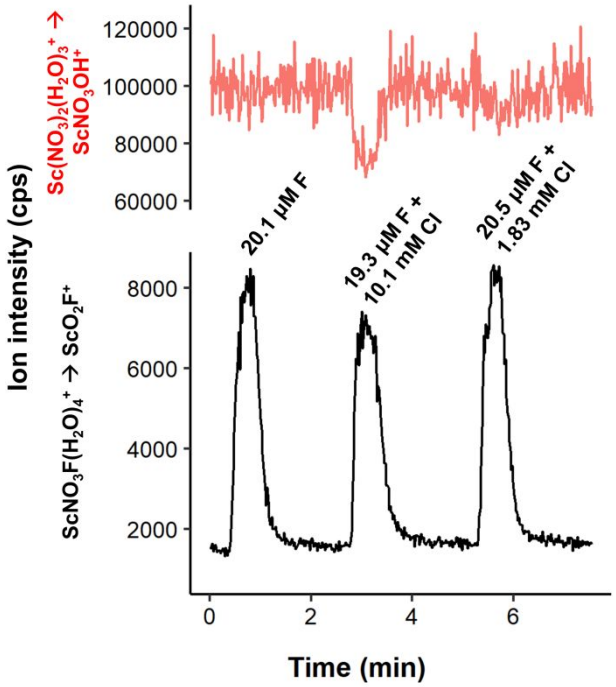

Figure 8. Flagging matrix effect by monitoring reagent ion $Sc(NO_3)_2(H_2O)_4^+$ (red) concurrently with analytical ion $ScNO_3F(H_2O)_3^+$ (black). An MS/MS detection mode was used where $ScNO_3F(H_2O)_4^+$ was fragmented to ScO_2F^+ at a collision energy of 45 eV and $Sc(NO_3)_2(H_2O)_3^+$ ion was fragmented to $ScOHNO_3^+$ using 35 eV collision energy. Integration times of 200 ms, and 500 ms, were used for reagent ion and analyte ion measurements, respectively. Flow injections of fluconazole samples were conducted with and without sucralose matrix. Data were acquired with a O_2 flow rate of 50 mL/min, and an interface air flow rate of 2.6 L/min.

Analytical considerations for post-plasma Sc-based ionization

While hydration of ions splits the analytical signal in the current experimental configuration, it is useful to consider the analytical characteristics to further contextualize the findings above. In Sc-based ionization, which offers the highest sensitivity in the above studies, the hydration distribution is narrow, effectively concentrating the analytical ions to $ScFNO_3(H_2O)_3^+$ and $ScFNO_3(H_2O)_4^+$ with near equal intensities. Consequently, the sensitivity of F detection using only $ScFNO_3(H_2O)_4^+$ (rather than summation of ion intensities for all hydrated ions) reaches 360 cps/(ng/mL) F. This value is two orders of magnitude larger than the highest sensitivity reported for F detection by ICP-MS techniques (Table 3) and comparable to that obtained by ICP-nanospray-MS using BaF^+ in our previous report.[16]

Table 3. Comparison of LODs and background equivalent concentrations (BECs) among various ICP-based mass spectrometric F detection techniques.

Technique	Ion or MS/MS Transition	Integration time (ms)	Sensitivity (cps/(ng/mL))	BEC (ng/mL F)	LOD (ng/mL F)
ICP-HRMS[8]	F^+	N/A[a]	0.026	2050	5070
ICP-MS/MS[11]	$BaF^+ \rightarrow BaF^+$	1000	3.2	607	43
ICP-MS/MS[13]	$BaF^+ \rightarrow BaF(NH_3)_3^+$	1000	1.6	21	22
ICP-MS/MS[12]	$BaF^+ \rightarrow BaF^+$	1000	2	400	60
ICP-MS[22]	BaF^+	9000	0.4	30	32
ICP-nanospray-MS[16]	BaF^+	500	281	191	11
ICP-nanospray-Orbitrap MS[5]	BaF^+	125	N/A[b]	112	7.6-21
This work ICP-nanospray-MS	$ScNO_3F(H_2O)_4^+$	500	360	357	19
This work ICP-nanospray-MS/MS	$ScNO_3F(H_2O)_4^+ \rightarrow ScO_2F^+$	500	14	120	16

a: a clear integration time for F was not reported in this study
b: The Fourier transform-based intensities in Orbitrap instrument are not directly comparable to those obtained using ion counting detectors in other techniques and therefore are not listed.

As noted in matrix effect studies above, hydration also results in increased possibility of isobaric interferences, necessitating use of MS/MS techniques. The MS/MS transition of $ScNO_3F(H_2O)_4^+ \rightarrow ScO_2F^+$ used in Cl matrix studies reduces the F detection sensitivity to 14 cps/(ng/mL). Despite this loss, the sensitivity is still 5-10 fold higher than that offered by recent ICP-MS methods using BaF^+ as analytical ion (Table 3). We note that the mass spectrometer used in our work is a dated equipment while modern instruments utilize larger ion sampling orifices and

axial field in collision cells, resulting in drastic improvements in ion transmission for MS/MS methods. Accordingly, improved sensitivities are expected even with hydration if more recent instruments are used. Increased sensitivity offered by post-plasma chemical ionization is important for measurement of transient signals (e.g. chromatographic detection) where shorter integration times are needed. Low sensitivities result in low absolute ion counts during the integration time, increasing the variation of signal because of counting statistics and reducing the precision of the measurements.[16] The data in Table 2 show that flow injection peak areas are measured with 5-8 RSD% for ~380 ng/mL injections at 500 ms integration time, indicating a reasonable performance for transient signal detection in our experiments even at the reduced sensitivity using MS/MS.

Table 3 also compares the LOD and background equivalent concentrations (BECs) in this work to other methods. The LODs in the present work were calculated by $3 \times SD_{baseline}$/sensitivity at 500 ms integration time. It is notable that post-plasma chemical ionization methods (denoted as ICP-nanospray) provide better LODs compared to ICP-MS methods in addition to higher sensitivities. The F BEC of 357 ng/mL in this work using $ScNO_3F(H_2O)_4^+$ without MS/MS is higher than 191 ng/mL in our previous work using post-plasma generated BaF^+,[16] likely because of hydration and increased probability of isobaric interferences.[5,16] Notably, the incorporation of MS/MS reduces BEC by a factor of 3. The corresponding improvement in LOD, however, is modest because of lowered sensitivity which reduces precision of baseline intensity measurements. As eluded above, use of more modern mass spectrometers with enhanced MS/MS capabilities is expected to further improve the LOD by increasing the ion flux and by enhancing the precision of measurements.

Overall, the promising performance of the post-plasma chemical ionization relative to ICP-MS methods, even with the extensive hydration, along with species-independent response and facile chromatographic coupling demonstrated in other works[5,16] underline the strengths and potential of this technique for quantitation of fluorochemicals.

Conclusions

The studies above shed light into details of post-plasma chemical ionization for F detection and offer insights to further improve its analytical performance. In particular, our investigations point to HNO_3 as a consequential species in post-plasma flow especially when the plasma is loaded with excess oxygen. Nitric acid's adverse effects can be rationalized via its reaction with F-containing ions, leading to neutralization and signal loss, or reactions with regent ions from nanospray, rendering them ineffective for ionization of HF. The effect is particularly severe for barium-based ionization where BaF^+ is used as analytical ion.

By using nanospray electrolytes with metal ions of higher charge and smaller ionic radius, greater robustness of F detection to HNO_3 is observed. The extent of robustness is quantified by measuring the fraction of reagent ions that are converted to F-containing ions per ng/mL of F injected into the ICP. We have observed the relative robustness to follow the order $AlNO_3F(H_2O)_n^+$ ~ $ScNO_3F(H_2O)_n^+$ > $LaFNO_3(H_2O)_n^+$ > $MgF(H_2O)_n^+$ > $BaF(H_2O)_n^+$. Notably, this order is analogous to the order of fluoride ion association constants with the metals in aqueous solutions. This similarity may potentially stem form role of hydration in gas phase ion-neural reactions, which remains to be further elucidated.

In terms of analytical performance, we observed the best balance of robustness and sensitivity using Sc-based ionization. This is partly imparted by higher intensities of Sc-containing ions generated by the nanospray and fewer species detected in the background at high oxygen

loads, thus concentrating the reagent ions into one major species. The matrix effects from Cl were greatly reduced using Sc-based ionization relative to Ba-based ionization, in line with better performance of Sc-based ionization at high oxygen levels.

Tolerance to HNO_3 offers ability to operate at high oxygen levels which has significant practical implications for coupling to chromatography. For gradient chromatography, the extent of carbon introduced into the plasma varies over the course of separation. Sensitivity of ionization to HNO_3 and oxygen load (e.g. using Ba-based ionization) requires a gradient of oxygen to be implemented with the solvent gradient to minimize HNO_3 formation.[5] However, a robust ionization in the presence of HNO_3 would enable use of a constant oxygen which greatly simplifies the operation.

In regards to specific features of chemical ionization, we have demonstrated that reagent ion monitoring provides a quality control metric to flag matrix effects without a prior knowledge or testing of the sample matrix. Finally, hydration was promoted in this study to gain fundamental insights into the ionization reactions. Yet, better LODs were obtained compared to recent ICP-MS/MS methods. Measures that reduce the hydration of the products (e.g. counterflow gas or higher temperatures in ion sampling) are expected to coalesce the hydration distribution, reducing isobaric interferences and improving sensitivity and detection limits.

Conflict of Interest Statement

Kaveh Jorabchi is co-inventor on issued and pandering patents and Samuel White is a coinventor on a pending patent related to the post-plasma chemical ionization technique investigated in this report.

Acknowledgements

This material is based upon work supported by the US National Science Foundation (NSF) under Grant CHE-1904835. We thank PerkinElmer for providing the ICP generator.

References

1 M. Inoue, Y. Sumii and N. Shibata, *ACS Omega*, 2020, **5**, 10633–10640.
2 P. Jeschke, in *Organofluorine Chemistry*, eds. K. Szabó and N. Selander, Wiley, 1st edn., 2021, pp. 363–395.
3 F. M. Rombach, S. A. Haque and T. J. Macdonald, *Energy Environ. Sci.*, 2021, **14**, 5161–5190.
4 J. L. Kyzer and M. Martens, *Chem. Res. Toxicol.*, 2021, **34**, 678–680.
5 F. A. Redeker, J. E. Lesniewski, G. Hahm, W. P. McMahon and K. Jorabchi, *Anal. Chem.*, 2022, **94**, 11865–11872.
6 D. R. Lide, *CRC Handbook of Chemistry and Physics*, 1992, vol. 268.
7 R. S. Houk, *Anal. Chem.*, 1986, **58**, 97A-105A.
8 X. Bu, T. Wang and G. Hall, *J. Anal. At. Spectrom.*, 2003, **18**, 1443–1451.
9 T. Egorova, R. Dietiker, B. Hattendorf and D. Günther, *Spectrochim. Acta, Part B*, 2012, **76**, 40–47.

10 N. L. A. Jamari, A. Behrens, A. Raab, E. M. Krupp and J. Feldmann, *J. Anal. At. Spectrom.*, 2018, **33**, 1304–1309.
11 N. L. A. Jamari, J. F. Dohmann, A. Raab, E. M. Krupp and J. Feldmann, *J. Anal. At. Spectrom.*, 2017, **32**, 942–950.
12 Y. Zhu, K. Nakano and Y. Shikamori, *Anal. Sci.*, 2017, **33**, 1279–1284.
13 W. Guo, L. Jin, S. Hu and Q. Guo, *J. Agric. Food Chem.*, 2017, **65**, 3406–3412.
14 S. Heuckeroth, T. N. Nxumalo, A. Raab and J. Feldmann, *Anal. Chem.*, 2021, **93**, 6335–6341.
15 J. E. Lesniewski, K. Zheng, P. Lecchi, D. Dain and K. Jorabchi, *Anal. Chem.*, 2019, **91**, 3773–3777.
16 S. White, K. Zheng, J. Tanen, J. E. Lesniewski and K. Jorabchi, *J. Anal. At. Spectrom.*, 2022, **37**, 870–882.
17 N. L. A. Jamari, J. F. Dohmann, A. Raab, E. M. Krupp and J. Feldmann, *Anal. Chim. Acta*, 2019, **1053**, 22–31.
18 R. E. Connick and M. S. Tsao, *J. Am. Chem. Soc.*, 1954, **76**, 5311–5314.
19 P. Becker and B. A. Bilal, *J. Solution Chem.*, 1985, **14**, 407–415.
20 G. Goldstein, *Anal. Chem.*, 1964, **36**, 243–244.
21 R. G. Parr and R. G. Pearson, *J. Am. Chem. Soc.*, 1983, **105**, 7512–7516.
22 W. Guo, X. Lin, L. Jin and S. Hu, *J. Agric. Food Chem.*, 2020, **86**, 103378.